Expert Systems with Applications 42 (2015) 3041–3047

Contents lists available at ScienceDirect

Expert Systems with Applications

journal homepage: www.elsevier.com/locate/eswa

Review

Digital image analysis for automatic enumeration of malaria parasites using morphological operations

J.E. Arco [d,*], J.M. Górriz [a,c], J. Ramírez [a,c], I. Álvarez [a,c], C.G. Puntonet [b,c]

[a] Department of Signal Theory Networking and Communications
[b] Department of Architecture and Computer Technology
[c] University of Granada, Granada 18071, Spain
[d] C/Periodista Daniel Saucedo Aranda S/N, C.P. 18071 Granada, Spain

ARTICLE INFO

Article history:
Available online 29 November 2014

Keywords:
Malaria parasites
Image analysis
Morphological operations
Adaptive histogram equalization
Adaptive thresholding

ABSTRACT

Every year, malaria kills between 660,000 and 1.2 million people, many of whom are children in Africa. The World Health Organization (WHO) encourages the development of rapid and economical diagnostic tests that allow for the identification of proper treatment methods. In this paper a novel method to automatically enumerate malaria parasites is proposed and evaluated, using a database consisting of 475 images with varying densities of malaria parasites. This method will analyze data by utilizing standard operations of image processing such as histogram equalization, thresholding, morphological operations and connected components analysis for parasite density estimation. The application of the proposed method yields an average accuracy rate of 96.46% with a low processing time of two seconds per image on a custom computing platform.

1. Introduction

Malaria has infected humans for over 50,000 years (Day, 2010). Epidemiological data show that somewhere in the world a child dies every 30 s because of this disease. This suggests that both vaccine development and the proper administration of available drugs are absolutely essential to treat malaria patients (O'Meara, Hall, & McKenzie, 2007a). A wrong diagnosis of this disease may have adverse clinical and therapeutic implications for patients and for endpoints of clinical trials of anti-malarial vaccines or drugs. Nowadays, there are a lot of different techniques for malaria diagnosis available in the market (Bhandari, Raghuveer, Rajeev, & Bandhari, 2008; Ngasala et al., 2008; Tangpukdee, Duangdee, Wilairatana, & Krudsood, 2009), but conventional microscopic examination remains the gold standard (Frean, 2010; Warhurst & Williams, 1996; Wongsrichanalai, Barcus, Muth, Sutamihardja, & Wernshorfer, 2013). Thus, the most important component of laboratory diagnosis is the quantification of parasite density. Accurate and replicable parasite counts are difficult to achieve because of inherent technical limitations and human inconsistency (Mitiku, Mengistu, & Gelaw, 2003). Digital image analysis provides an opportunity to improve the performance of parasite density quantification, decreasing the time required to count the parasites and avoiding bias from human error.

A technique was proposed (Díaz, González, & Romero, 2009) for quantifying erythrocytes in stained thin blood films. The image was corrected from luminance differences and the normalized RGB color space was used for classifying pixels as erythrocyte or background followed by an Inclusion-Tree representation that structures the pixel information into objects. Finally, a two step classification process identifies infected erythrocytes, using a trained bank of classifiers. The main drawback of this approach is that it needs user intervention, which results in time consuming and large inter and intra-observer variabilities (Alexander, Schellenberg, Ngsala, Petzold, & Drakeley, 2010).

Automatic parasite detection has been addressed in Abdulnasir, Mashor, and Mohamed (2013), Das, Ghosh, Pal, Maiti, and Chakraborty (2012), Frean (2009), Moon et al. (2013) and Tek, Dempster, and Kale (2006, 2010). In Makkapati and Rao (2009), a scheme based on HSV color space is presented. This method was focused on detecting dominant hue range and calculating optimal saturation thresholds. The dominant color in this kind of images is representative of the background, so dividing the hue range of 360° into six 60° segments enables to find the number of pixels that fall within each hue segment and thus, the dominant range of color. Optimal saturation thresholds were identified by using the method proposed in Otsu (1979). This automatic thresholding method is

* Corresponding author. Tel.: +34 958241285.
E-mail addresses: jearco@correo.ugr.es (J.E. Arco), gorriz@ugr.es (J.M. Górriz), javierrp@ugr.es (J. Ramírez), illan@ugr.es (I. Álvarez), carlosgp@ugr.es (C.G. Puntonet).

http://dx.doi.org/10.1016/j.eswa.2014.11.037
0957-4174/

widely used in classic image segmentation applications (Guo, Wang, & Xia, 2014; Vala & Bashi, 2013; Yang, Shen, Long, & Chen, 2012) and is based on selecting the discriminant criterion, so as in order to maximize the separability of the resulting classes in gray levels. This technique was found to give an optimal threshold for bimodal distributions but did not work well for unimodal distributions. Precisely, the blood smear images present unimodal distributions due to the fact that most of the pixels belong to the background, and only a little bit of them are pixels from parasites, resulting in a histogram with only a big and wide peak.

In further studies, granulometric estimation and morphological techniques were employed with promising outcomes (Khatri, Ratnaparkhe, Agrawal, & Bhalchandra, 2013). A method (di Ruberto, Dempster, Khan, & Jarra, 2001) introduced a morphological approach to cell segmentation, which was more accurate than the classical watershed-based algorithm (Bieniek & Moga, 2000). A hemispherical disk-shaped structuring element was used to enhance the roundness and the compactness of the red cells, while a disk-shaped flat structuring element was used to separate overlapping cells. Regarding the classification step, two different methods were used, one based on morphological operator (Díaz-Huerta, Felipe-Riveron, & Zetina, 2014; González & Woods, 2002) and another one based on color histogram similarity (Colombo, Rizzi, & Genovesi, 1997; del Bimbo, Mugnaini, Pala, & Turco, 1998). Despite the brilliant solutions presented by these approaches, these kind of techniques were very sensitive to the image quality. Besides, the fact that it is necessary to analyze both the hue and the saturation images makes the process slow down, although morphological operations will be used by our approach in a different way.

In this study an image processing technique, which is not used on conventional algorithms, is proposed, focusing on a low time consumption and obtaining good results independently of the variability of the images. Fig. 1 shows a block diagram of the proposed algorithm for enumerating parasites. Firstly, the acquired image (a gray-scale image, not an RGB or HSV) is preprocessed by means of a low pass filtering that removes noise, and an adaptive histogram equalization that corrects the contrast of the images to improve its quality. Once this is achieved, the adequate threshold to binarize the image is estimated. In our method, an adaptive thresholding based scheme allows an effective classification of pixels. This means that the election of whether a pixel belongs to the background or to the signal (parasites and white blood cells) is only established by the pixels around it, that is its neighborhood. Then, morphological methods (regional minimum and closing operation) use granulometries to evaluate the area of the connected components, labeling the components belonging to parasites and counting the number of them.

The organization of the rest of the paper is as follows. Details or our method based on adaptive processing and morphological operations are mentioned below. The method consist of four stages. In Section 2.1 the preprocessing step is explained. This consists of a Gaussian low-pass filter to reduce the noise of the image and an adaptive histogram equalization with the objective of achieving an image with more contrast. Then, in Section 2.2 we focus on an adaptive thresholding process that allows an automatic binarization of an image dividing the entire image into small subimages and applying different equalizations to each one. Section 2.3 explains different operations based on the so-called mathematical morphology. These operations are capable of filling the holes in parasites created in previous steps and eliminating all the elements in the image that are smaller than the structural element. In Section 2.4, a measurement of the properties of the regions are made, resulting in labeling and subsequent classification (parasites or white blood cell) as based on this measure. The experimental results are provided in Section 3, and a discussion of research contributions and practical advantages in addition to the conclusions are available in Section 4.

2. Image processing

2.1. Preprocessing

The aim of the preprocessing stage is to obtain images with more contrast than the original image. This process consists of two operations to increase the contrast of the raw acquired images: image filtering to mitigate noise and image enhancement, in the form of histogram equalization. In this paper, we are interested in filtering operations that are performed directly on the pixels of an image. That is why the term *spatial filtering* is used to differentiate this type of process from the more traditional frequency domain filtering. Generally, the linear spatial filtering of an image f whose size is $M \times N$, using a $m \times n$ mask, is given by the following function:

$$g(x,y) = \sum_{s=-a}^{a}\sum_{t=-b}^{b} w(s,t) f(x+s, y+t) \tag{1}$$

where ω's are mask coefficients. To generate a completely filtered image, this equation must be applied to $x = 0, 1, \ldots M-1$ and $y = 0, 1, \ldots, N-1$, where $a = (m-1)/2$ and $b = (n-1)/2$.

In this stage, a Gaussian low-pass filter is applied to the input image to get clear signal regions and suppress the influence of noise. Fig. 2 shows the result of convolving a Gaussian mask with the original image. After Gaussian filter, the image is brighter than the original one, thus the intensities of the pixels are higher than they were before. This means that the process of choosing a threshold

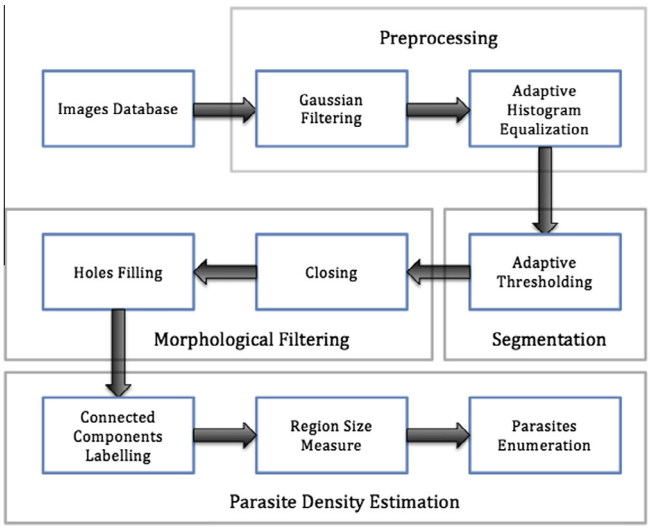

Fig. 1. Image processing steps.

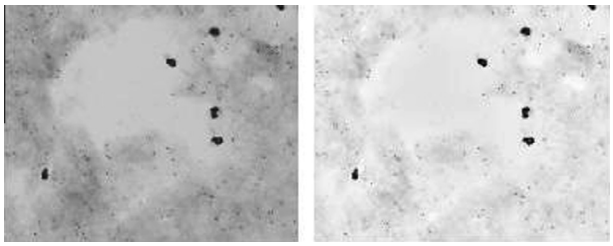

Fig. 2. Left side: original image. Right side: image after Gaussian Filtering.

to segment the image will become easier, thus the intensity differences between signal pixels (parasites) and background have been increased.

The next step in preprocessing is histogram equalization. This operation spreads out intensity values along the total range of values in order to achieve higher contrast. This method is especially useful when an image is represented by close contrast values, such as images in which both the background and foreground are bright at the same time, or else both are dark at the same time. However, slow speed and the overenhancement of noise it produces in relatively homogeneous regions are two problems. In order to solve them, an adaptive histogram equalization has been used Pena (2010). It differs from ordinary histogram equalization in the respect that the adaptive method computes several histograms, each corresponding to a distinct section of the image, and uses them to redistribute the lightness values of the image. The optimal value of the size of each image subdivision has been determined, being 64 pixels (8×8), and a bilinear interpolation of the border pixels of two subdivisions is calculated. Therefore, in order to prevent the noise overamplification a contrast limitation is used (Zuiderveld, 1994).

Fig. 3 shows the result of the adaptive histogram equalization. At first, it is necessary to identify the most important histogram sections. From all the millions of pixels in the image, only a very small percentage are of any interest: parasites and white blood cells. The blue ellipsis indicates the location of these pixels. The peak, which represents the background, has been shifted to the right compared to its position in the original image. This means that the background pixels now have higher intensities, so that there is a bigger difference between the background and signal pixels intensities. In turn, the selection of the desired threshold used to convert the image to binary form is simplified.

Before segmentation, another operation (called h-minima transform) (Samboal, 2012) is used. It effectively suppresses all intensity minima in the image whose difference with its neighbor is less than a threshold called depth. With this operation, the difference between the background pixels are reduced. The depth parameter of the algorithm is experimentally tuned finally selecting the value of 0.01.

2.2. Segmentation

Thresholding is one of the widely methods for image segmentation (Al-Amri, Kalyankar, & Khamitkar, 2010). It is useful in discriminating foreground from the background. By selecting an adequate threshold value T, the gray level image can be converted to binary image. In this way, thresholding can be seen as an operation that involves testing a function T as found in the following form:

$$T = T[x, y, p(x, y), f(x, y)] \tag{2}$$

where $f(x, y)$ is the gray level of the pixel (x, y) and $p(x, y)$ denotes some local property of this pixel. The most common way to convert a gray-level image to a binary image is to select a single threshold value (T), defined as follows:

$$g(x, y) = \begin{cases} 1 & \text{if } f(x, y) > T \\ 0 & \text{if } f(x, y) \leqslant T \end{cases} \tag{3}$$

Then all the gray level values below this T will be classified as black (0), and those above T will be white (1).

The segmentation problem becomes one of selecting the proper value for the threshold T. A frequent method used to select T is by analyzing the histograms of the type of images that want to be segmented. In the first place, Otsu's method (Otsu, 1979) is used. This is a nonparametric and unsupervised method for automatic thresholding. An optimal threshold is selected by the discriminant criterion so as to maximize the separability of the resulting classes in gray levels. The ideal case is when the histogram presents only two dominant modes and a clear valley (bimodal). In this case the value of T is selected as the valley point between the two modes. But the histograms of the images in the database are more complex, with many peaks and not clear valleys, and it is not always easy to select the value of T. That is the reason why the local characteristics of the image are utilized through a process called *adaptive thresholding* (Rodríguez, 2010).

First, the average image is calculated, that is, the image is convolved with a mean filter (15×15 mask). Although this is usually used as a smoothing operation it is not what is intended in this case. Then, the average image is compared with the value of each pixel in the input image. Therefore, there are two possibilities, as shown here:

- If the pixel in the original image is greater than T% of the pixel in the average image, then pixel is labeled as 1 and it therefore belongs to the background.
- If the pixel in the original image is less than T% of the pixel in the average image, then the new value of this pixel is labeled as 0. Therefore, it belongs to the signal.

Although the parameter T has always the same value, the segmentation threshold varies with each of the images, since T is a percentage, that is, depends on the intensities of the pixels in the image, which is the reason that this method works quite well: it adapts to the local characteristics of each image. The proposed method is very robust to the variation of this parameter, so that it is not difficult to choose an appropriate value, which works well for all images. Fig. 4 shows the result of this operation. There, the background is now completely uniform (white), while both malaria parasites and white blood cells are black pixels. Further-

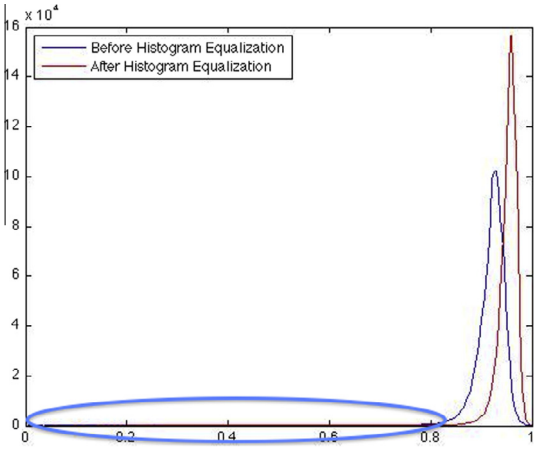

Fig. 3. Comparison between histogram before and after equalization.

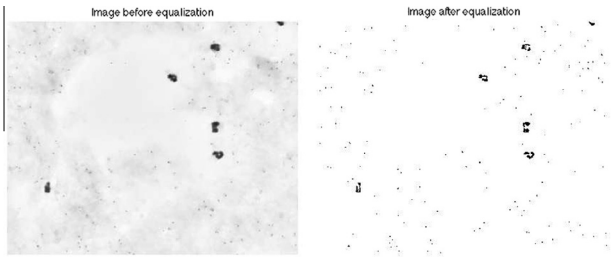

Fig. 4. Left side: image before thresholding. Right side: binary image.

more, the selected threshold gives very good results. A value too small would eliminate many parasites. On the other hand, a high value would unduly increase the number of parasites because such pixels would be considered as parasites belonging to the background.

2.3. Morphological filtering

When the image is binarized, it will be treated to obtain the only information of real importance, the ability to extract the desired components of an image. For this, the tools of the so-called *mathematical morphology* (Jones & Svalbe, 1994) is used. There are two primary operations namely, dilation and erosion. The former has mainly the application of filling holes. The latter eliminates irrelevant details in the image. Eqs. (4) and (5) show operational definitions in formal mathematical terms:

$$A \oplus B = \{z|(\widehat{B})_z \cap A \subseteq A\}. \quad (4)$$

$$A \ominus B = \{z|(B)_z \subseteq A\} \quad (5)$$

The dilation of A and B is the set of all the shifts, z, such that $\widehat{B}$ and A overlap in at least one element. The erosion of A and B is the set of all the pixels z such that B has to be contained in A. In both operations a *structural element* (van den Boomgard & van Balen, 1992) is required that moves across the image in the same way as a convolution (González & Woods, 2002).

Combining dilation and erosion a more complex filtering is obtained. *Closing* (Vincent, 2004), which is a dilation followed by an erosion, tends to smooth contour sections, but it generally fuses narrow breaks and long thin gulfs, eliminates small holes and fills gaps in the contour (Alba, Martín, Cide, & Mora, 2006). Fig. 5 shows the result of this operation. In this image a set of pixels can be seen that represent a white blood cells. As discussed below, it is necessary to measure characteristics of the sets of pixels to differentiate between parasites and white blood cell. For this reason, the gaps in all these sets must be filled so that the measures obtained are reliable.

Opening generally smoothes the contour of an object, breaks narrows isthmuses, and eliminates thin protrusions. Though the main application in this study is to eliminate all the elements in the image that are smaller than the structural aspects of the selected element. In the next section the results achieved with this operation will be reported.

2.4. Connected components analysis

The connected components analysis of a binarized image consists of labeling (Alnuweiri & Kumar, 1991) those pixels having a value '1' as seen in white. This is followed by a measurement of the properties of the region resulting in labeling and subsequent classification as based on this measure. The procedure follows that the same identification tag will be assigned to all pixels that have a binary value '1' and which are connected by a path of pixels also with value '1'. The label is the unique index that indicates the region to which the pixels belong to. To get the most efficient results, an algorithm based on run-length encoding has been used with the following operations. First, a Run-Length encoding (RLE) of the input image (Ronse & Devijver, 1984) is applied. After this, a preliminary tagging is used, keeping the label equivalencies or connected regions with different label in a table of local matches. Then, the resolution of the equivalences tables is done, relabeling of the sequences based on the resolved equivalence classes.

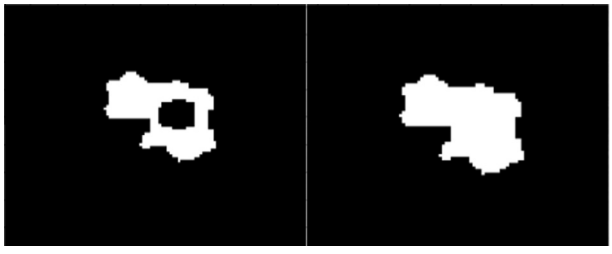

Fig. 5. Left side: image before closing operation. Right side: image after closing.

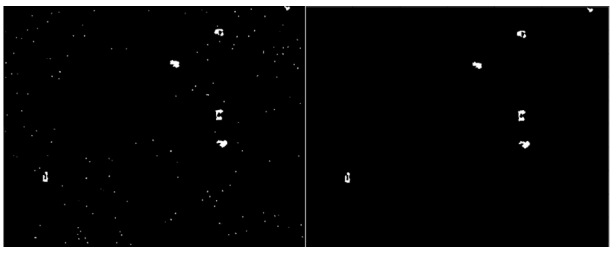

Fig. 6. Left side: image before opening operation. Right side: image after opening.

Once the binary image is separated into its corresponding connected components, each of these different properties is measured. Given that, the main difference between white blood cells and malaria parasites is their size, so that is the property to be measured. Then, all region areas (number of pixels forming the area) are checked, and based on the results, it is divided into parasites or white blood cells. In this way, the higher value label assigned to a region shows the total number of regions (parasites and white blood cells) existing in the image. Finally, the opening operation is used in order to eliminate the white blood cells, presenting a picture in which there are only parasites. The size of the structural element has been selected to be equal to the average size of a white blood cell, so that all elements smaller than those are removed. This obtains an image with only white blood cells (see Fig. 6). By calculating the difference between both of the images, then the objective of this work (see Fig. 7) is obtained.

3. Results and discussion

Errors in parasite density estimation by conventional microscopy are common, and apart from possibly deleteriously influencing the management of individual patients, have the potential to produce major consequences for clinical efficacy trials of malaria vaccines (O'Meara, Hall, & McKenzie, 2007b) or prophylactic drugs (Frean & Dini, 2007). In this study, highly accurate manual counts of a range of parasite densities made it possible to experiment extensively with digital counting methods, and to critically evaluate particle analysis algorithms. Figs. 8 and 9 show a comparison between the manual count and digital counts obtained by the process developed in this paper. In the first image, the number of parasites in each of the images is measured, while the second shows

Fig. 7. Result of all the processing.

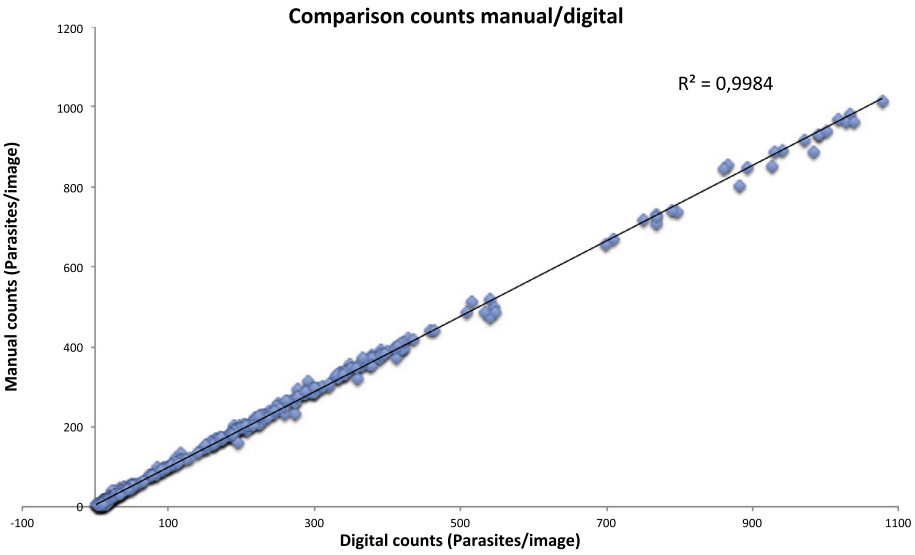

Fig. 8. Linear regression of digital counts on manual counts of 475 images.

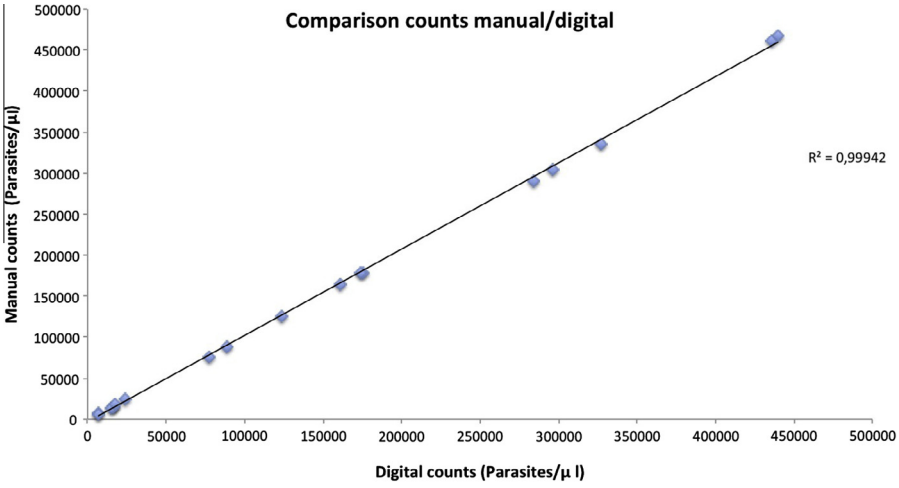

Fig. 9. Linear regression of aggregated digital counts on manual counts of 19 slides.

parasite density, as measured by the number or parasites per μl, for each of the patients. Both Figs. 8 and 9 show the linear regression to visually establish the correlation between the values obtained using the manual and digital methods.

Generally, digital and manual counts are well correlated, whereas the conventional counting provides significantly lower results than the other two methods (see Table 1). This is due to the fact that in conventional counting of relative numbers of parasites and leukocytes, human operator biases, which are absent in the digital and manual counts, presumably account for this to underestimate parasite densities. Fig. 8 shows the correlation between digital and manual counting in each of the images of the database, obtaining a linear regression coefficient of $R^2 = 0.9984$. There is also a correlation between parasite densities obtained by each of the two methods, with a linear regression coefficient of $R^2 = 0.99942$.

Another important is the fact that there is no relationship between accuracy and parasite densities, providing good results both for images with a smaller number of them (low signal/noise ratio) and images with a high number of parasites (therefore, high SNR). There is also a comparison between the results obtained in this paper and the results obtained by other systems capable of

Table 1
Comparison of manual, digital, and conventional parasite density estimations.

Slide	Number of parasites counted per slide		Parasite density, as parasites per μl		
	Manual	Digital	Manual	Digital	Conventional
BF3A	5022	4955	125161	123491	109725
BF5A	4516	4438	178410	175328	152178
BF6A	10686	10082	461853	435747	271600
BF7A	9373	9166	290682	284263	200083
BF8A	344	358	6908	7189	5834
BF9A	634	664	15756	16501	11359
BF10A	1003	1082	15343	16551	18638
BF13A	2446	2478	76501	77501	50110
BF18A	22477	21158	467219	439801	429400
AMI3a	424	424	23887	23887	17500
AMI32	5819	5667	178360	173701	125000
BF7Ab	8059	7857	303762	296148	200083
BF8Ab	291	299	6701	6885	5834
BF9Ab	369	394	14033	14983	11359
BF13Ab	1373	1369	88951	88691	50110
BF15A	3904	3816	164379	160673	144050
BF17A	6807	6642	335219	327093	238467
AMI3b	281	255	18891	17143	17500
Total	83828	81104	2772016	2685576	2008720

Table 2
Comparison of manual, John Frean's, and proposed method for parasite density estimation.

Image	Number of parasites per slide			Discrepancy (%)	
	Manual	Frean	Proposed	Frean	Proposed
BF3A	5022	5071	4955	0.981	1.33
BF5A	4516	4540	4438	0.53	1.72
BF6A	10686	10438	10082	2.32	5.65
BF7A	9373	9515	9166	1.51	2.2
BF8A	344	289	358	15.99	4.07
BF9A	634	619	664	2.37	4.73
BF10A	1003	870	1082	13.26	7.87
BF13A	2446	2158	2478	11.76	1.30
BF18A	22477	21956	21158	2.32	5.86
AMI3a	424	438	424	3.30	0
AMI32	5819	6149	5667	5.67	2.61
BF7Ab	8059	8259	7857	2.38	2.5
BF8Ab	291	277	299	4.81	2.75
BF9Ab	369	333	394	9.76	6.77
BF13Ab	1373	1356	1369	1.24	0.29
BF15A	3904	3914	3816	0.26	2.25
BF16A	14265	14273	13739	0.06	3.68
BF17A	6807	6999	6642	2.82	2.42
AMI3b	281	272	255	3.2	9.25
Average				4.45	3.54

digitally counting parasites. Table 2 shows these results. Under this proposed method, the average error is 3.54%, within the limits recommended by the WHO, while in the case of Frean (2010), the average error is 4.45%. Therefore, the variance of these errors has been calculated, obtaining a more efficient estimator: 6.15 in the case of the proposed method and 21.07 in Frean (2009) method. Still, this is not the only important point. The key is in the processing time of each image. Frean proposes a system that requires from 5 to 10 min to get the results for each patient (with 25 images per patient). The system proposed in this paper is able to obtain the digital count in 50 s, (using a laptop with Core-i5 Processor with a clock speed of 2.3 GHz), with no detectable increasing in computing time in images with high parasite densities.

4. Conclusions

In the current study, we have developed an image analysis software which could potentially be employed for the routine determination of parasitemia from thick blood films. The design of this software is based on several steps. The preprocessing step involves the enhancement of the image using an adaptive histogram equalization. The next step, the binarizing process, is focused on the adequate selection of a threshold that divides the image in two groups: signal (white blood cells and parasites) and background pixels. Lastly, the use of morphological operations (regional minimum and closing) evaluate the area of the connected components, getting only the parasites and counting the number of them.

Approaches such as histogram equalization, morphology or thresholding have been employed to estimate the number of malaria parasites in thick blood films. However, such approaches are unable of precisely determining the number of parasites. To accurately and rapidly quantify the number of parasites in digital images, we employed a novel approach where the key steps are adaptive histogram equalization and adaptive thresholding. The first one is based on the matching of the histogram of all the images to a reference one, reducing the variability of the images. In this way, a extraction of important information from images with very different characteristics is performed, so it is necessary to evaluate a single image instead of three (in RGB or HSV space) as some approaches do, with the serious costs in processing speed that it entails. As regards the selection of a threshold to segment the images, Otsu's method (widely used in literature) does not get good results due to the nature and features of the images. Furthermore, the use of a global threshold is meaningless because the wide range of grayscale intensities and images complexity makes impossible to segment an image with only one threshold for the entire one. The adaptive thresholding technique proposed on this work choose an individual threshold for each group of each pixels (called neighborhood) attending to the local features of them, significantly improving the accuracy of the algorithm and showing better results than other approaches.

In two situations, we noticed that certain particularities of the images would lead to a false interpretation of parasites and thus, an increasing in discrepancy between manual and digital counts. The first one is related with Giemsa-stain, which is used to differentiate nuclear morphology of white blood cells and malaria parasites. In some images, the quantity of Giemsa-stain is too high and there are not important differences between their grayscale intensities and parasites intensities. But if besides this stain pixels located almost adjacent to parasites, histogram equalization process would probably equalize their intensities, with the improper increasing in the number of parasites this could cause. Another problem that should be improved in a future update is related with very high parasites density images. Sometimes parasites are close together and morphological operations are not capable of segmenting them. This could be solved by using morphological operations both before and after the thresholding step, and not only after it. Another suggestion for future research might be the adaptation of the algorithms used in this work to smartphones. Malaria occurs mostly in poor areas of the world and this kind of devices are not as expensive as laptops or PCs, in addition to doctors could diagnose and choose the correct treatment anywhere and not only in specialized laboratories.

The aim of this work was the development of a new method for enumeration of malaria parasites that improved the problems of other approaches and it has been broadly achieved. The experiments carried out on the database composed by 475 images yielded a value of accuracy equal to 96.46%, a variance of these errors equal to 6.15 and needing 2 s per image, which outperformed the algorithm proposed in Frean (2009), with a value of accuracy equal to 95.55%, variance of errors equal to 21.07 and needing 18 s per image. Adaptive processing techniques are the key in this work, being able to overcome the variability in images, extracting local information and making different decisions in each region of the image. We come to the conclusion that local and adaptive processing is a powerful tool that might be very useful not only for the diagnosis of malaria disease, but also in other digital images processing fields such as computer vision or patterns recognition.

References

Abdul-nasir, A. S., Mashor, M. Y., & Mohamed, Z. (2013). Colour image segmentation approach for detection of malaria parasites using various color models and k-means clustering. *Biology and Medicine, 1*.

Al-Amri, S. S., Kalyankar, N. V., & Khamitkar, S. D. (2010). Image segmentation by using threshold techniques. *Journal of Computing, 2*.

Alba, J. L., Martín, F., Cide, J., & Mora, I. (2006). *Aplicación a procesado de imágenes binarias y monocromáticas*.

Alexander, N., Schellenberg, D., Ngsala, B., Petzold, M., & Drakeley, C. (2010). Assessing agreement between malaria slide density readings. *Malaria Journal, 9*, 4.

Alnuweiri, H., Kumar, V. (1991). Fast image labeling using local operators on mesh-connected computers. In *IEEE transactions on pattern analysis and machine intelligence*.

Bhandari, P. L., Raghuveer, C. V., Rajeev, A., & Bandhari, P. D. (2008). Comparative study of peripheral blood smear, quantitative buffy coat and modified centrifuged blood smear in malaria diagnosis. *Indian Journal of Pathology and Microbiology, 51*, 108–122.

Bieniek, A., & Moga, A. (2000). An efficient watershed algorithm based on connected components. *Pattern Recognition, 33*, 907–916.

Colombo, C., Rizzi, A., & Genovesi, I. (1997). Histogram families for color-based retrieval in image databases. *ICIAT*, 204–211.
Das, D. K., Ghosh, M., Pal, M., Maiti, A. K., & Chakraborty, C. (2012). Machine learning approach for automated screening of malaria parasite using light microscopic images. *Micron, 45*, 97–106.
Day, W. M. (2010). *Malaria*.
del Bimbo, A., Mugnaini, M., Pala, P., & Turco, F. (1998). Visual querying by color perceptive regions. *Pattern Recognition, 31*(9).
Díaz, G., González, F. A., & Romero, E. (2009). A semi-automatic method for quantification and classification of erythrocytes infected with malaria parasites in microscopic images. *Journal of Biomedical Informatics, 42*, 296–307.
Díaz-Huerta, C. C., Felipe-Riveron, E. M., & Zetina, L. M. M. (2014). Quantitative analysis of morphological techniques for automatic classification of micro-calcifications in digitized mammograms. *Experts Systems with Applications, 41*, 7361–7369.
di Ruberto, C., Dempster, A., Khan, S., & Jarra, B. (2001). Analysis of infected blood cell images using morphological operators. *Image and Vision Computing, 20*, 133–146.
Frean, J. (2009). Reliable enumeration of malaria parasites in thick blood films using digital image analysis. *Malaria Journal*.
Frean, J. (2010). Microscopic determination of malaria parasite load: Role of image analysis. *Microscopic: Science, Technology, Applications and Education*.
Frean, J., Dini, L. (2007). Quality assessment of malaria laboratory diagnosis in south africa. World Health Organization: Policy and Procedures of the WHO/INICD Microbiology External Quality Assessment Programme in Africa Geneva: WHO.
González, R. C., & Woods, R. E. (2002). *Digital image processing*. Prentice-Hall. ISBN: 0-201-18075-8.
Guo, W. Y., Wang, X. F., & Xia, X. Z. (2014). Two dimensional Otsu's thresholding segmentation method based on grid box filter. *Optik, 125*, 5234–5240.
Jones, R., & Svalbe, I. (1994). *Basis algorithms in mathematical morphology*. *Advances in electronics and electron physics*. Academic Press.
Khatri, K. M., Ratnaparkhe, V. R., Agrawal, S. S., & Bhalchandra, A. S. (2013). Image processing approach for malarial parasite identification. *IJCA*, 0975–8887.
Makkapati, V. V., & Rao, R. M. (2009). Segmentation of malaria parasites in peripheral blood smears images. *Acoustics, Speech and Signal Processing*, 1361–1364.
Mitiku, K., Mengistu, G., & Gelaw, B. (2003). The reliability of blood film examination for malaria at the peripheral health unit. *Ethiopian Journal of Health Development, 17*(3), 197–204.
Moon, S., Lee, S., Kim, H., Freitas-Junior, L. H., Kang, M., Ayong, L., et al. (2013). An image algorithm for malaria parasite stage classification and viability quantification. *Plos one, 8*(4), e61812.
Ngasala, B., Mubi, M., Warsame, M., Petzold, M. G., Massele, A. Y., Gustafsson, L. L., et al. (2008). Impact of training in clinical and microscopy diagnosis of childhood malaria on antimalarial drug prescription and health outcome at primary health care level in Tanzania: A randomized controlled trial. *Malaria Journal, 7*, 199.
O'Meara, W. P., Hall, B. F., & McKenzie, F. E. (2007a). Malaria vaccine efficacy: The difficulty of detecting and diagnosing malaria. *Malaria Journal*.
O'Meara, W. P., Hall, B. F., & McKenzie, F. E. (2007b). Malaria vaccine efficacy: The difficulty of detecting and diagnosing malaria. *Malaria Journal*.
Otsu, N. (1979). A threshold selection method from gray-level histograms. In *IEEE Transactions on systems, MAN, and cybernetics* (Vol. 9).
Pena, C. J. V. (2010). Ahe (ecualización del histograma adaptativo).
Rodríguez, E. J. V. (2010). Precisión de la microscopía óptica en microfluídica. Aplicaciones (Ph.D. thesis). Universidad de Extremadura.
Ronse, C., & Devijver, P. A. (1984). Connected components in binary images: the detection problem. Research studies.
Samboal, M. M. (2012). Detección de células cancerosas en imágenes de neoplasia intraepitelial cervical (nic).
Tangpukdee, N., Duangdee, C., Wilairatana, P., & Krudsood, S. (2009). Malaria diagnosis: a brief review. *Korean Journal of Parasitology, 2*, 93–102.
Tek, F. B., Dempster, A. G., & Kale, I. (2006). Malaria parasite detection in peripheral blood images. *BMVC*, 1–10.
Tek, F. B., Dempster, A. G., & Kale, I. (2010). Parasite detection and identification for automated thin blood film malaria diagnosis. *Computer Vision and Image Understanding, 114*, 21–32.
Vala, H. J., & Bashi, A. (2013). A review on Otsu image segmentation algorithm. *IJARCET, 2*, 2.
van den Boomgard, R., van Balen, R. (1992). Methods for fast morphological image transforms using bitmapped images. In *Computer vision, graphics, and image processing: graphical models and image processing* (Vol. 55, pp. 252–254).
Vincent, L. (2004). *Morphological area openings and closings for greyscale images*. *Shape in Picture: Mathematical Description of Shape in Grey-Level Images*. Springer-Verlag. chapter.
Warhurst, D. C., & Williams, J. E. (1996). Laboratory diagnosis of malaria. *Journal of Clinical Pathology, 49*, 533–538.
Wongsrichanalai, C., Barcus, M. J., Muth, S., Sutamihardja, A., & Wernshorfer, W. H. (2013). A review of malaria diagnostic tools: Microscopy and rapid diagnostic test (rdt). *American Journal of Tropical Medicine and Hygiene, 77*, 119–127.
Yang, X., Shen, X., Long, J., & Chen, H. (2012). An improved median-based Otsu image thresholding algorithm. *AASRI Procedia, 3*, 468–473.
Zuiderveld, K. (1994). Contrast limited adaptive histogram equalization. In *Graphic gems IV* (pp. 474–485). San Diego: Academic Press.